Advanced Sensor Research

WILEY | ADVANCED SENSOR RESEARCH Open Access

www.advsensorres.com

RESEARCH ARTICLE OPEN ACCESS

Electronic Nose for Indoor Mold Detection and Identification

Hankun Yang[1,2] | Martin Sommer[2] | Stephanie Bauer[3] | Uli Lemmer[1,2]

[1]Light Technology Institute (LTI), Karlsruhe Institute of Technology (KIT), Karlsruhe, Germany | [2]Institute of Microstructure Technology (IMT), Karlsruhe Institute of Technology (KIT), Eggenstein-Leopoldshafen, Germany | [3]Domatec GmbH, Mühldorf a. Inn, Germany

Correspondence: Uli Lemmer (uli.lemmer@kit.edu)

Received: 18 August 2025 | **Revised:** 28 October 2025 | **Accepted:** 10 November 2025

Keywords: chemiresistive | electronic nose | linear discriminant analysis | machine learning | mold detection

ABSTRACT

Indoor mold infestations lead to adverse effects on air quality and thus pose significant health risks to humans. Traditional methods for mold detection and identification are time-consuming and costly. In this study, the application of an electronic nose as a highly reliable tool for detecting and identifying mold is explored. Two common indoor mold species, *Stachybotrys chartarum* and *Chaetomium globosum*, each separately grown on two different substrates, are investigated. Our e-nose uses vapor-liquid-solid-grown, UV-activated SnO_2 nanowires as the chemiresistive sensing material. Linear discriminant analysis (LDA) is used for classification. Moreover, novelty detection is enabled by default using decision boundaries. While the conventional LDA only shows mediocre classification results, improved versions can achieve an average F1-score of 98.37%. Therefore, our results demonstrate that the e-nose can not only detect but also identify different mold genera, and thus making a significant step toward fast, objective, and cost-effective indoor air quality monitoring.

1 | Introduction

Mold fungi are commonly found in damp indoor environments and can pose a variety of health issues for humans and animals. In addition to direct health risks, the resulting remediation costs and long-term consequential damage can represent a significant financial burden. Therefore, timely mold detection and identification are crucial for maintaining a healthy indoor environment and preventing costly consequences. Two filamentous fungi, *Stachybotrys chartarum* and *Chaetomium globosum*, are particularly interesting because they are among the most frequently detected molds in damp and water-damaged indoor environments, especially on cellulose-based construction materials such as gypsum board and wallpaper [1–3]. Both species are representative of distinct ecological and biochemical groups relevant to indoor exposure assessment [1–5].

S. chartarum is a slow-growing, cellulolytic mold that requires high water activity and sustained moisture to proliferate. Certain chemotypes produce macrocyclic trichothecenes (e.g., satratoxins) and spirocyclic drimanes, metabolites implicated in irritant and inflammatory responses [4, 6–10]. *S. chartarum* is repeatedly isolated from gypsum wallboard and other cellulose-rich indoor substrates in situ [1–3].

By contrast, *C. globosum* is a rapidly growing, cellulolytic fungus that commonly colonizes paper, wood, and gypsum materials in water-damaged buildings [1, 11]. Field surveys consistently report *C. globosum* among the most abundant genera on moisture-compromised building materials [1, 2, 5].

Traditional methods for mold detection and identification are based on various sampling techniques such as swab, tape, bulk, and air samples, followed by culture-based laboratory analyses

[12]. These approaches typically require three to seven days, leading not only to delays in remediation but also to additional costs. An alternative approach is the use of mold-detection dogs. They detect and locate mold by the characteristic odor the mold produces. However, they have significant limitations: their training is costly and time-consuming [13], and while they can signal the presence of mold, they lack the ability to differentiate between different mold genera, making precise identification difficult if not practically impossible.

To retain the fundamental principle of odor-based mold detection, electronic noses (e-noses) emerge as a promising technological solution, that enables rapid, cost-efficient, and objective detection. E-noses usually consists of a sensor array that is used to generate an odor-specific signal pattern. This pattern can be recognized using various machine learning algorithms [14]. Multiple sensing principles exist, including, among others, mechanical (e.g. surface-acoustic-wave) and electrical (e.g. capacitive, resistive, and field-effect-based). Its capability of detecting and distinguishing biological samples is further documented by existing reports in related applications such as food safety [15–17], and medical [18]. Various classification methods can be used, such as neural networks, decision trees, ensembles, principal component analysis, and linear discriminant analysis (LDA). While the best classifier is usually application-dependent, LDA stands out as a good and versatile general method. Moreover, a decision boundary can be implemented that can be directly utilized for novelty detection [19], which is critical for practical e-nose applications where previously unknown odors may be presented. Other studies also demonstrated the successful use of e-noses to identify various mold genera based on their typical odor profiles [20, 21]. For mold detection and identification specifically, the sensing mechanism of the e-nose relies on the sensing of volatile organic compounds (VOCs) emitted as metabolic byproducts by the mold. These VOCs include a range of alcohols, ketones, ethers, and esters. Depending on the VOC, it may directly act as an oxidizing or reducing gas or indirectly affect the adsorption properties of other interacting gases such as oxygen species [22]. For instance, *S. chartarum* is known to emit unique microbial volatile organic compounds (MVOCs) such as anisole (methoxybenzene), 3-octanone, and various alcohols [3, 23]. Furthermore, the VOC profile can vary depending on the substrate and incubation period, influencing the mold's metabolic expression. Likewise, *C. globosum* has been shown to produce various metabolites with 3-ocatnone, 2-pentatnone, and 1-hexanol as the top three hexane-soluble fraction [24]. Additionally, it produces a diverse array of secondary metabolites, including chaetoglobosins, azaphilones, and chaetomugilins, which are relevant in the context of indoor exposure and bioactivity [11, 25]. The differences in MVOC output can be captured by the e-nose, leading to identification of and separation between mold species [26].

Here, we report a detailed evaluation of the potential of a chemiresistive e-nose system for the detection and identification of the two mold species, *S. chartarum* and *C. globosum*, by using linear discrimination analysis (LDA). We additionally explore different strategies to improve the classification performance. Furthermore, two different growth substrates are used to simulate different environments and test the generalization capability of the e-nose.

2 | Results and Discussion

2.1 | Transient Response

To assess the ability of an e-nose to detect and identify distinct mold species on different substrates, measurements under laboratory conditions are conducted. Besides the reference air, bare growth substrates (agar mixed with shredded gypsum and wheat flour) are measured as additional reference samples. All four combinations between mold and substrates are considered as distinct classes and are measured individually. The experimental details are stated in the Experimental Section. The transient resistance responses of *S. chartarum* (a) and *C. globosum* (b) are shown in Figure 1. The average resistance for reference air is approximately 30 kΩ. Sample measurements start with an initial spike in resistance, followed by a steadily falling signal throughout the whole 30 min measurement duration. The response signal of the samples does not fully stabilize in this time frame. In contrast, the resistance values recover rapidly when presented with reference air. Over the course of two weeks, only minor signal changes were observed, as shown in Figure S3. The sub-sensors are showing negative humidity coefficients, as expected for SnO_2, which is an n-type semiconductor.

2.2 | Conventional Linear Discriminant Analysis

First, the classification performance of a conventional LDA model is assessed. For that, the LDA model is trained and tested with all seven initially defined classes. The number of discriminants $\boldsymbol{t} \in [1..\boldsymbol{n_c} - 1]$, is optimized. Hereby, $\boldsymbol{n_c}$ is the number of classes.

In this case, with seven classes, $\boldsymbol{t}$ is found to be six. Additionally, feature selection is performed iteratively to remove features with a negative impact on the classification. This can be interpreted as ignoring bad sub-sensors. Here, two from the initial 16 features are removed, while the remaining 14 sensor signals are considered for further processing.

Training (dots) and test (crosses) data are shown in Figure 2a, which are projected to the discriminant space (d1, d2). Except for SoW (pink) and CoW (purple), all other classes overlap severely in the displayed discriminant space. Nonetheless, the majority of data can still be distinguished by the LDA as shown in the confusion matrix (Figure 2b) and the classification report (Table S2), partially due to the contribution of other discriminants. The no-mold samples (A, G, W) have a substantial number of misclassifications among each other and thus have lower F1-scores than all other classes containing mold. In contrast, SoW and CoW display the highest F1-scores (> 94%) with 100% precision. SoW and CoW both have 100% precision, with no other classes being misclassified as these two. This finding aligns with the observations in the LDA plot in Figure 2a. A non-negligible part of the test data is classified as novelty by this LDA model, most prevalently of the classes A and CoW, indicating a higher signal noise or deviation. Practically, the LDA can classify all seven classes, although the performance is lackluster. Therefore, various performance-improving approaches are shown in the following subsections. This conventional LDA model, including all seven classes, is abbreviated to LDA-0 to distinguish it from other models.

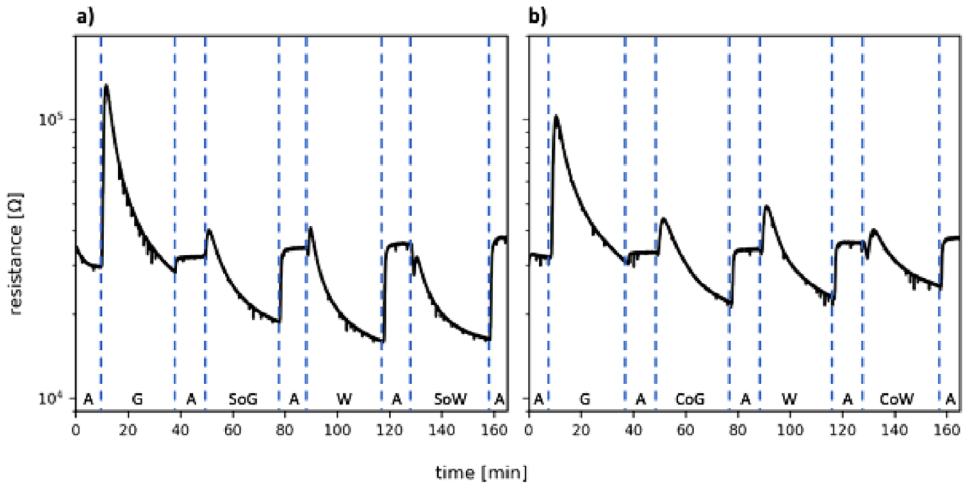

FIGURE 1 | Two representative measurement series showing the median signal of the 16 subsensors. a) Measurement containing *S. chartarum* samples, b) Measurement containing *C. globosum* samples. The segments are abbreviated as follows: reference air (A), gypsum reference (G), wheat reference (W), *S. chartarum* on gypsum (SoG) and wheat (SoW), *C. globosum* on gypsum (CoG) and wheat (CoW).

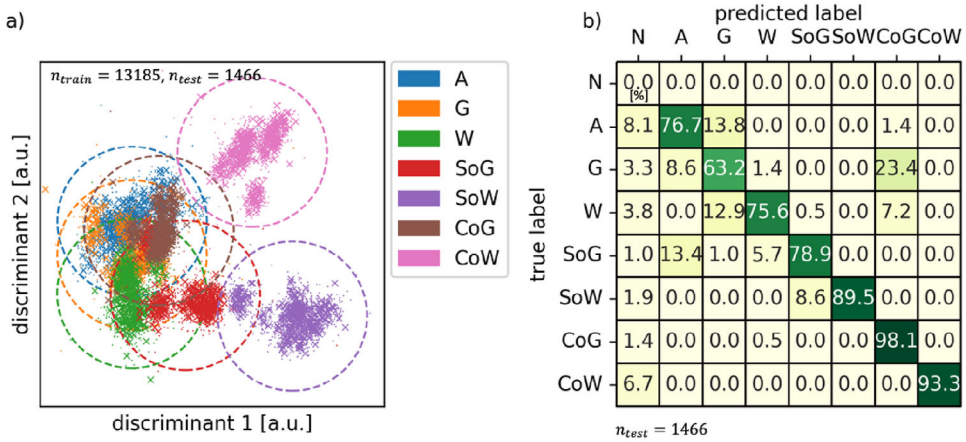

FIGURE 2 | Classification results of the conventional LDA including all 7 classes. a) Projected data points in the discriminant space (d1, d2). Training data are displayed as dots, and the test data are displayed as crosses. The classes are abbreviated as follows: novelty (N), reference air (A), gypsum reference (G), wheat reference (W), *S. chartarum* on gypsum (SoG) and wheat (SoW), *C. globosum* on gypsum (CoG) and wheat (CoW). The decision boundaries of each class are shown as dashed lines in the same color as the represented class.

2.3 | Substrate-Independent Analysis

Mold detection and identification are the two most important tasks. The LDA model can be simplified to solely focus on these tasks by removing the substrate dependency of the classes. To remove this dependency, the classes A, G, and W are merged as "no mold" (NM), SoG and SoW are merged as *Stachybotrys* (S), and CoG and CoW are merged as *Chaetomium* (C). This substrate-independent model is subsequently abbreviated as LDA-SI.

The optimized number of discriminants is found to be $t = 2$. Seven features are selected from the 16 initial features. The resulting LDA plot is shown in Figure 3a. In there, the three classes display less severe overlap compared to the LDA-0 model. The NM class has data outside its own and inside other classes' decision boundaries, which leads to misclassifications that are evidenced by the corresponding confusion matrix in Figure 3b. This also causes the lower recall values of other classes in the classification report in Table S3. *S. chartarum* has a single out-of-bound data cluster, which is positioned at the center of the NM class.This is reflected by misclassifications to NM in the confusion matrix. The data points of *C. globosum* are well enclosed within its decision boundary with a negligible number of outliers. Therefore, the recall of *C. globosum* is over 99%. All metric values of *C. globosum* are higher than the corresponding ones of *S. chartarum*. Compared to the LDA-0 model, novelty is rarely predicted. This finding indicates that the mold is mainly responsible for the detectable odor signal, while substrates have a lesser impact.

2.4 | Substrate-Specific Analysis

In a real-world application case, the growth substrate is usually known beforehand. Therefore, simplified substrate-specific LDA models can be created that exclude all other substrate references

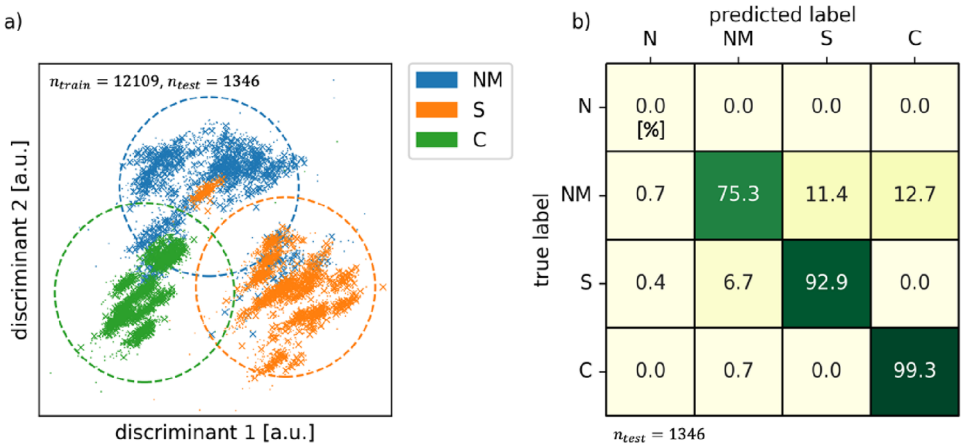

FIGURE 3 | Substrate-independent LDA model test results. a) LDA plot b) Confusion matrix normalized to rows (true labels). The classes are abbreviated as follows: novelty (N), no mold (NM), *S. chartarum* (S), and *C. globosum* (C). The decision boundary (DB) is shown as dashed lines in the LDA plot.

and mold-on-substrate samples, which in our case results in two models: the gypsum-specific (LDA-G) and the wheat-specific (LDA-W) model. Both substrate-specific models are generalized as LDA-SS.

For both LDA-G and LDA-W, the optimal number of discriminants is found to be $t = 2$. From the 16 features, nine are selected for LDA-G and eight for LDA-W. The LDA plot of LDA-G (Figure 4a) shows less overlap compared to LDA-0. The spatial separation is even superior in the LDA plot of LDA-W, as shown in Figure 4c. Here, all three classes are well enclosed within their respective decision boundaries, and no overlapping of the decision boundaries is observed.

Compared to the LDA-SI model (refer to Figure 3a), the NM class has fewer outliers, which translates into a significant increase in recall for both LDA-SS models, as shown in Table S4. On gypsum, the *S. chartarum* class has a considerably higher precision (98.59 %) compared to recall (87.87%). This is attributed to the misclassification as NM evidenced in the confusion matrix (Figure 4b). Still, a non-negligible part of NM class test data is predicted as novelty for both LDA-SS models. Both LDA-G and LDA-W achieve higher average F1-scores (92.64% and 98.09% respectively) compared to LDA-0 and LDA-SI. These findings generally support a substrate-specific approach, if possible.

2.5 | LDA Ensemble With Softmax Regressor

In our analysis, we have observed that individual LDA models that are trained on specific subsets of classes may perform significantly better; for example, the substrate-specific models discussed in section 2.4. Thus, this behavior is exploited by creating an ensemble of LDA models, each trained with a unique subset of classes. The detailed model structure is shown in Figure 5. This means for a given number of classes n_c, $n_m = 2^{n_c} - n_c - 1$ number of models are initially created, as deduced in Equation S1. Thereafter, a softmax regressor takes the n_m predictions as input and re-predicts one of the n_c classes. This LDA-ensemble with a subsequent softmax regression is subsequently abbreviated as LDA-SR.

Undesirably, the softmax regressor intrinsically removes the novelty detection function of the LDA models. Therefore, an additional majority voting algorithm is implemented to reintroduce the novelty class. The softmax prediction is accepted if more than half of the relevant LDA models in the ensemble match. Otherwise, the prediction is rejected and declared novel.

The LDA ensemble is trained without any hyperparameter optimization or feature selection for the individual LDA models. Hereby, always the maximum number of discriminants is used. Next, the softmax regressor is tuned and trained using the LDA model predictions of the training data. The optimal regularization strength C is found to be 0.09. Feature selection is performed on the pre-prediction of the LDA ensemble and removes 20 from the initial 120 features. This can be interpreted as removing bad-performing LDA models from the ensemble. Finally, the complete LDA-SR model is tested. The confusion matrix of the test result without majority voting is shown in Figure 6a, and the classification report is presented in Table S5. The model achieves superb precision, recall, and thus also F1-scores across all classes. No significant misclassification is observed. As expected, majority voting reintroduces the novelty label if enabled, as shown in the confusion matrix in Figure 6b. But only a minor amount of novelty is detected during testing. No recall value changes occur from the majority voting, since majority voting only introduces the novelty label, which has no occurrences in the test data set. Compared to LDA-0, LDA-SI, and LDA-SS, all classification performance metrics improved considerably. This is especially significant for low-performing classes; hence, the performance disparity between classes decreases. It must be noted that compared to other presented models, the LDA-SR is more computationally expensive for large class counts n_c due to the exponentially growing number of LDA models $n_m \propto 2^{n_c}$ in the ensemble. This drawback can be partially mediated by feature selection and by reducing the number of classes, for example, with the simplification approaches discussed in sections 2.3 and 2.4.

It should be noted that in a real-world application, other sources of VOC, such as building materials, human activities, household

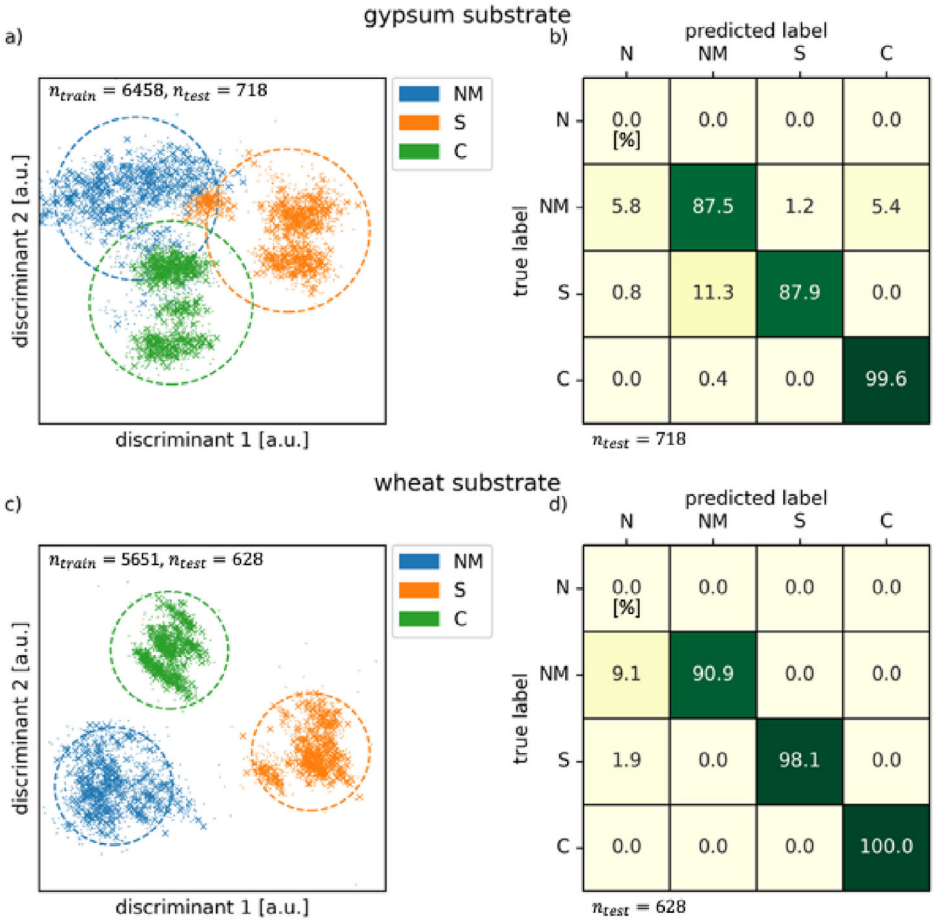

FIGURE 4 | Substrate-specific analysis results. a) and c): LDA plots, b) and d): confusion matrices for gypsum and wheat-specific models, respectively. The classes are abbreviated as follows: novelty (N), no mold (NM), *S. chartarum* (S), and *C. globosum* (C). The decision boundary (DB) is shown as dashed lines in the LDA plots.

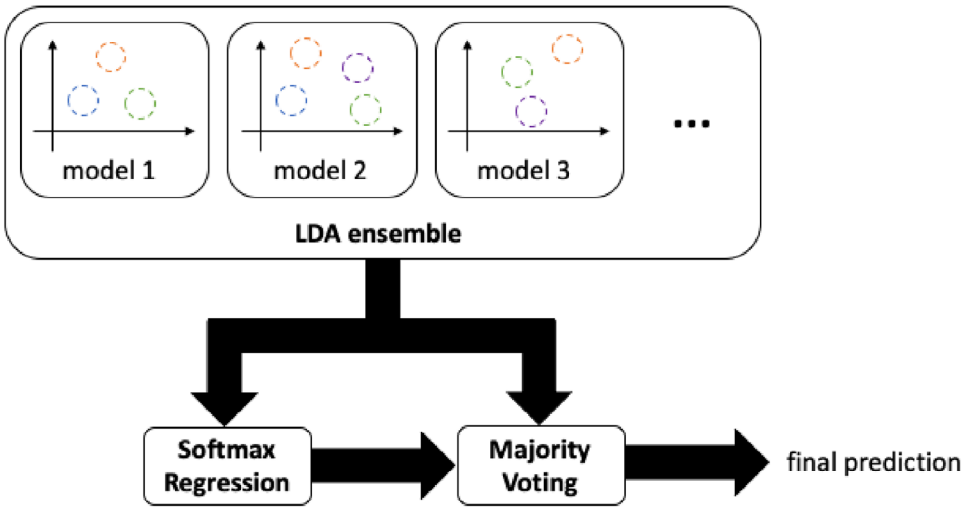

FIGURE 5 | Data flow chart of the ensemble classifier including multiple LDA models, a softmax regressor, and a majority voting algorithm.

products, and combustion by-products, have to be considered [26–29]. Consequently, the e-nose may face challenges sensing mold, depending on the concentration and type of the interfering VOCs. Nevertheless, local baseline measurements at mold-free areas should at least enable mold indication using outlier detection methods. Other environmental factors, such as humidity and airflow, can be relatively easily controlled even for mobile devices. Finally, the e-noses ability to detect other common mold genera such as *Aspergillus* and *Penicillium* is considered likely since they also emit characteristic MVOCs [30–32]. But additional research is required to establish which mold species can be unambiguously and reliably identified and which species belong to broader

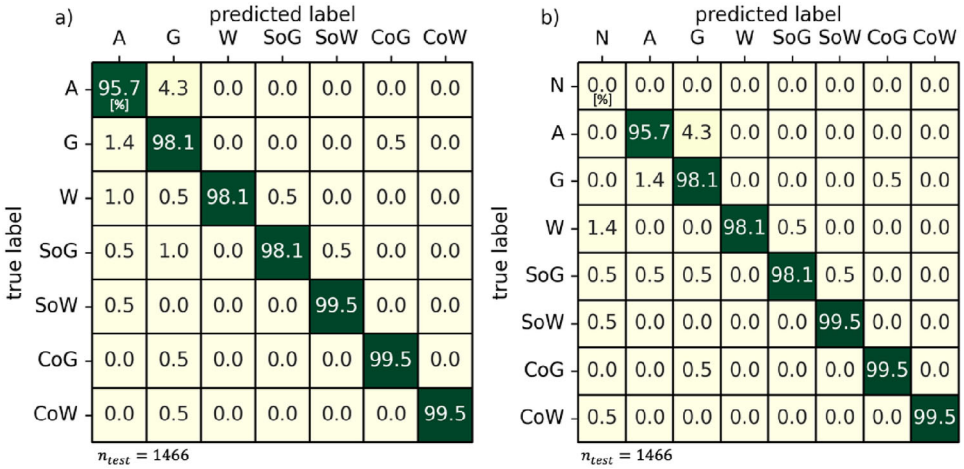

FIGURE 6 | Confusion matrices of the test result of LDA ensemble combined with softmax regression. a) without majority voting, b) with majority voting. The classes are abbreviated as follows: novelty (N), reference air (A), gypsum reference (G), wheat reference (W), *S. chartarum* on gypsum (SoG) and on wheat (SoW), *C. globosum* on gypsum (CoG) and on wheat (CoW).

groups where individuals within the group are indistinguishable from each other.

3 | Conclusion

This work assesses the capability of a chemiresistive e-nose sensor to detect and identify common indoor mold. For that, the two mold species, *S. chartarum* and *C. globosum*, are chosen and grown in laboratory conditions on two different substrates (agar mixed with either shredded gypsum or wheat). An e-nose using UV-activated, chemiresistive SnO_2 nanowires is used for this case. Different LDA variations are trained and tested using the measurement data. The conventional LDA model (LDA-0), which is trained on all seven initial classes, only displays mediocre results with an average F1-score of 83.74% due to severe overlapping of decision boundaries. Therefore, different strategies are explored to improve the classification performance. The LDA model can be simplified by either merging classes to remove the substrate dependency (LDA-SI) or by creating LDA models specific to each substrate (LDA-SS). Both approaches lead to improvements in classification performance. Moreover, a novel ensemble classifier consisting of individual LDA models and a subsequent softmax regressor (LDA-SR) is implemented and tested. This ensemble is further extended by a majority voting algorithm to preserve the novelty detection capability of the LDA models. This LDA-SR model achieves an astounding F1-score of 98.57% in testing with all seven classes. Conclusively, we show that the chemiresistive e-nose can successfully and highly reliably detect and identify the presented mold genera grown on two different substrates.

4 | Experimental Section

4.1 | Mold Sample Preparation

All fungal strains used in this work were obtained from the State Health Authority of Baden-Wuerttemberg (Germany) and cultivated under standardized laboratory conditions as detailed below. To ensure optimal growth conditions for the selected mold species, two different culture media were used: whole wheat flour agar (composition: 30 g whole wheat flour, 15 g agar-agar, 1000 mL distilled water), and gypsum board agar (composition: 30 g finely ground gypsum board, 15 g agar–agar, 1000 mL distilled water). For the whole wheat flour agar, flour and agar–agar were first weighed, then mixed with distilled water, and finally autoclaved (Varioclav 135S, HP Labortechnik GmbH) at 121°C for 15 min to ensure sterility. For the gypsum board agar, gypsum board was first mechanically ground into a fine powder, then mixed with agar-agar, and subsequently dissolved in distilled water. Finally, the mixture was autoclaved under identical conditions as the whole wheat flour agar. Each culture medium was aliquoted into sterile culture bottles (DURAN 1000 mL, GLS 80, DWK Life Sciences) under sterile conditions. After cooling to room temperature, the agar solidified, forming a stable growth surface. After complete solidification of the media, the culture bottles were inoculated with the selected mold strains. The mold species *S. chartarum* and *C. globosum* were cultured separately in different bottles. Each sterile bottle was inoculated in a Class II biological safety cabinet (Airstream ESCO Class II Biological Safety Cabinet) to prevent cross-contamination. The spores were applied directly onto the surface of the agar media using a sterile loop. Subsequently, the inoculated bottles were incubated at 25 ± 3°C with 60% relative humidity. The incubation time was at least 10 days or until the agar surface was fully colonized by mold. Regular visual and microscopic inspections were conducted to monitor the growth phase and ensure full colonization.

4.2 | Sensor Fabrication

A suitable sensing material is required to operate a chemiresistive sensor. For this purpose, tin(IV) oxide (SnO_2) nanowires (NWs) were chosen for their well-known superb gas sensing capabilities [33–54]. The SnO_2 NWs were manufactured by the vapor-liquid-solid (VLS) process, as described in references [54, 55]. First, a ceramic boat was filled with two spatula tips of the precursor tin(II) oxide (SnO) powder. The precursor-filled boat was placed in the center of the tube oven with an inner diameter of

approximately 40 mm. Growth substrates (Si-wafers) are placed immediately after the precursor boat in the gas flow direction on top of a second ceramic boat. The surface of the Si-wafers had been sputtered with 5 nm Au to enable the VLS process. The oven tube was first evacuated and heated to 300°C in the first step to remove remaining residues and impurities. In a second step, the temperature was raised to 1040°C over 2 h and then kept for 2 h. During this step, the pressure inside the tube was maintained at 300 mbar and 50 sccm Ar and 0.1 sccm O_2 flows were constantly supplied for the VLS process. Finally, the substrates were allowed to cool down slowly overnight. A detailed illustration of the VLS setup is shown in Figure S1a, and an electron micrograph of the obtained SnO_2 NWs is shown in Figure S1b. Only SnO_2 NWs were used as the sensing material in our sensor. The chemiresistive e-nose platform used in this work was designed in-house at Karlsruhe Institute of Technology (KIT) and has been successfully employed in the past for various projects [54, 56]. It is inspired by the preceding "Karlsruhe Mikronase" (KAMINA) sensor [15, 49, 57–63]. The sensing area of the platform consists of an interdigitated electrode array. Each of the 17 gold electrodes in the array is 50 µm wide and 50 µm apart from its next neighbor. The overlapping length of the electrodes is 4 mm. SnO_2 NWs were dispersed in 2-propanol by magnetic stirring and were subsequently deposited on top of the electrodes by mask-assisted drop casting. The SnO_2 NWs electrically connected the electrodes to form 16 chemiresistive sub-sensors. Images of the sensor area before and after deposition are shown in Figure S2. The sensor was operated at room temperature (24 ± 3°C) and the SnO_2 NWs were excited using UV irradiation ($\lambda = 365$ nm, $I \approx 15\ mW\ cm^{-2}$) to promote gas-material interactions and to reduce the electrical resistivity of SnO_2. Per measurement cycle, the electrical resistances of all 16 sub-sensors were captured and logged. The entire cycle is executed approximately once per second.

4.3 | Experimental Setup

A zero-air generator (Sylatech, TG 12 UP) was used to obtain clean and dry reference air. The reference air was humidified to 90% relative humidity (RH) in a controlled manner. This was achieved by redirecting and fully humidifying 90% of the reference air with a washing bottle before merging and remixing it back with the remaining 10% dry reference air.

The rationale for using 90% RH is detailed below. The substrates had a high capacity for water storage. When the carrier gas humidity was too low, such as at 50% RH, the stored water was released into the carrier gas. This release caused two critical issues. First, the substrates dried out over time, severely altering the environmental conditions. Second, the reabsorbed humidity in the carrier gas resulted in an enormous resistance difference between reference air and the other measurements. For example, when using reference air at 50% RH, it was observed that the resistance for the reference air was around 10 MΩ. In contrast, resistances around 10 kΩ were observed for other gas flows. Furthermore, the absolute noise of the reference air measurements was also in the MΩ range. Therefore, the reference air's difference and noise overshadowed the relatively minor resistance differences between the samples, subsequently impairing the classification. By increasing the relative humidity to 90%, these issues were mitigated.

The humidified reference air was either directly used for reference measurement via the bypass or rerouted to the samples as carrier gas. Each measurement consisted of alternating segments of reference air and samples. The measurements always started and ended with a reference air measurement. All sample measurements were 30 min long, while the reference air measurements had a measurement time of 10 min. The shorter reference air measurement duration was justified due to faster signal stabilization compared to sample measurements. For each mold species, eight measurements were taken over the course of two weeks.

4.4 | Data Analysis

The following seven distinct base classes were defined and labeled: reference air (A), gypsum reference (G), wheat reference (W), *S. chartarum* on wheat and gypsum substrate (SoW and SoG), and *C. globosum* on wheat and gypsum substrate (CoW, CoG). Each sample consisted of 16 features, which are the resistance values from the sub-sensors. Only data from the last 5 min of each measurement segment was extracted to obtain the most stationary and stable signal. Across all measurements, 158 091 samples were taken. The data was resampled for each second by linear interpolation that results in 323 770 total samples. 36 595 of these data were labeled. A more detailed class-dependent distribution of the labeled samples is presented in Table S1. The number of data samples per class varied due to the different number of measurement segments per class. Such imbalanced data sets may negatively impact the performance of machine learning models generally and also of LDA specifically [64–67]. For this reason, the data was randomly downsampled so that the sample size of each class matches the minority class (2107 data samples). Logarithm to the base of 10 is applied to all resistance feature values. No further preprocessing was performed. Although the data at this stage only loosely conform to a normal distribution according to QQ-plots, the deviations were tolerable for subsequent analyses [68]. The data was shuffled and split into training and test data with a relative test size of approximately 10%. For all LDA models, the decision boundaries are calculated using f-distribution with a fixed confidence interval of 95% according to Henrion and Henrion [19]. The number of used discriminants was optimized using ten-fold cross-validation, if not otherwise stated. Feature selection was iteratively done by backward elimination of features. The metrics confusion matrix, precision, recall, and F1-score were evaluated for the test results. Python (3.13.0) was used for all data analysis with the following packages used for calculations numpy (2.1.3), scipy (1.14.1), sklearn (1.5.2) and imblearn (0.13.0). For all random processes the random_state variable was set to 42 for repeatability.

Funding

The authors gratefully acknowledge the Deutsche Forschungsgemeinschaft (DFG, German Research Foundation) under Germany's Strategy via the Excellence Cluster 3D Matter Made to Order (3DMM2O, EXC-2082/1-390761711) for financial support.

Conflicts of Interest

The authors declare no conflicts of interest.

Data Availability Statement

The data that support the findings of this study are available from the corresponding author upon reasonable request.

References

1. I. Došen, K. F. Nielsen, G. Clausen, and B. Andersen, "Potentially Harmful Secondary Metabolites Produced by Indoor *Chaetomium* Species on Artificially and Naturally Contaminated Building Materials," *Indoor Air* 27 (2017): 34–46, https://doi.org/10.1111/ina.12290.

2. D. Méheust, P. Le Cann, G. Reboux, L. Millon, and J.-P. Gangneux, "Indoor Fungal Contamination: Health Risks and Measurement Methods in Hospitals, Homes and Workplaces," *Critical Reviews in Microbiology* 40 (2014): 248–260, https://doi.org/10.3109/1040841X.2013.777687.

3. D. A. Betancourt, K. Krebs, S. A. Moore, and S. M. Martin, "Microbial Volatile Organic Compound Emissions From *Stachybotrys chartarum* Growing on Gypsum Wallboard and Ceiling Tile," *BMC Microbiology* 13 (2013): 283, https://doi.org/10.1186/1471-2180-13-283.

4. D. M. Kuhn and M. A. Ghannoum, "Indoor Mold, Toxigenic Fungi, and *Stachybotrys chartarum*: Infectious Disease Perspective," *Clinical Microbiology Reviews* 16 (2003): 144–172, https://doi.org/10.1128/CMR.16.1.144-172.2003.

5. M. J. Mendell, A. G. Mirer, K. Cheung, M. Tong, and J. Douwes, "Respiratory and Allergic Health Effects of Dampness, Mold, and Dampness-Related Agents: A Review of the Epidemiologic Evidence," *Environmental Health Perspectives* 119 (2011): 748–756, https://doi.org/10.1289/ehp.1002410.

6. R. A. Etzel, E. Montaña, W. G. Sorenson, G. J. Kullman, T. M. Allan, and D. G. Dearborn, "Acute Pulmonary Hemorrhage in Infants Associated with Exposure to *Stachybotrys atra* and Other Fungi," *Archives of Pediatrics & Adolescent Medicine* 152 (1998): 757–762, https://doi.org/10.1001/archpedi.152.8.757.

7. J. J. Pestka, I. Yike, D. G. Dearborn, M. D. W. Ward, and J. R. Harkema, "*Stachybotrys Chartarum*, Trichothecene Mycotoxins, and Damp Building–Related Illness: New Insights Into a Public Health Enigma," *Toxicological Sciences* 104 (2008) 4–26, https://doi.org/10.1093/toxsci/kfm284.

8. M. A. Hossain, M. S. Ahmed, and M. A. Ghannoum, "Attributes of *Stachybotrys chartarum* and its Association With Human Disease," *Journal of Allergy and Clinical Immunology* 113 (2004): 200–208, https://doi.org/10.1016/j.jaci.2003.12.018.

9. M. Mahmoudi and M. E. Gershwin, "Sick Building Syndrome. III. *Stachybotrys chartarum*," *Journal of Asthma* 37 (2000): 191–198, https://doi.org/10.3109/02770900009055442.

10. M. R. Fogle, D. R. Douglas, C. A. Jumper, and D. C. Straus, "Growth and Mycotoxin Production by *Chaetomium Globosum*," *Mycopathologia* 164 (2007): 49–56, https://doi.org/10.1007/s11046-007-9023-x.

11. V. Dwibedi, S. K. Rath, S. Jain, et al., "Key Insights Into Secondary Metabolites From Various *Chaetomium* Species," *Applied Microbiology and Biotechnology* 107 (2023): 1077–1093, https://doi.org/10.1007/s00253-023-12365-y.

12. R. T. Niemeier, S. K. Sivasubramani, T. Reponen, and S. A. Grinshpun, "Assessment of Fungal Contamination in Moldy Homes: Comparison of Different Methods," *Journal of Occupational and Environmental Hygiene* 3 (2006): 262–273, https://doi.org/10.1080/15459620600637333.

13. R. Griffith, K. Jayachandran, W. Whitstine, and K. Furton, "Differentiation of Toxic Molds via Headspace SPME-GC/MS and Canine Detection," *Sensors* 7 (2007): 1496–1508, https://doi.org/10.3390/s7081496.

14. D. Karakaya, O. Ulucan, and M. Turkan, "Electronic Nose and Its Applications: A Survey," *International Journal of Automation and Computing* 17 (2020): 179–209, https://doi.org/10.1007/s11633-019-1212-9.

15. V. Y. Musatov, V. V. Sysoev, M. Sommer, I. Kiselev, M. Pardo, and G. Sberveglieri, "Close-To-Practice Assessment of Meat Freshness with Metal Oxide Sensor Microarray Electronic Nose," in AIP Conference Proceedings (AIP, 2009) 469–472, https://doi.org/10.1063/1.3156585.

16. W. Jia, G. Liang, H. Tian, J. Sun, and C. Wan, "Electronic Nose-Based Technique for Rapid Detection and Recognition of Moldy Apples," *Sensors* 19 (2019): 1526, https://doi.org/10.3390/s19071526.

17. R. Sánchez, F. Pérez-Nevado, I. Montero-Fernández, J. Lozano, F. Meléndez, and D. Martín-Vertedor, "Application of Electronic Nose to Discriminate Species of Mold Strains in Synthetic Brines," *Frontiers in Microbiology* 13 (2022): 897178, https://doi.org/10.3389/fmicb.2022.897178.

18. K. de Heer, S. I. Vonk, M. Kok, et al., "eNose Technology can Detect and Classify Human Pathogenic Molds In Vitro: A Proof-of-Concept Study of *Aspergillus fumigatus* and *Rhizopus oryzae*," *Journal of Breath Research* 10 (2016): 036008, https://doi.org/10.1088/1752-7155/10/3/036008.

19. R. Henrion and G. Henrion, *Multivariate Datenanalyse* (Springer Berlin Heidelberg, 1995), https://doi.org/10.1007/978-3-642-57792-5.

20. Z. Suchorab, M. Frąc, Ł. Guz, et al., "A Method for Early Detection and Identification of Fungal Contamination of Building Materials Using E-Nose," *PLoS One* 14 (2019): e0215179, https://doi.org/10.1371/journal.pone.0215179.

21. D. Majerek, G. Łagód, V. Kočí, and R. Černý, "Density-Based Clustering of E-Nose Output From Mold-Contaminated Buildings," *AIP Conference Proceeding* 2429 (2021): 020021, https://doi.org/10.1063/5.0070164.

22. V. Shah, J. Bhaliya, G. M. Patel, and P. Joshi, "Room-Temperature Chemiresistive Gas Sensing of SnO2 Nanowires: A Review," *Journal of Inorganic and Organometallic Polymers and Materials* 32 (2022): 741–772, https://doi.org/10.1007/s10904-021-02198-5.

23. P. Gao and J. Martin, "Volatile Metabolites Produced by Three Strains of *Stachybotrys chartarum* Cultivated on Rice and Gypsum Board," *Applied Occupational and Environmental Hygiene* 17 (2002): 430–436, https://doi.org/10.1080/10473220290035462.

24. R. Kumar, A. Kundu, A. Dutta, S. Saha, A. Das, and A. Bhowmik, "Chemo-Profiling of Bioactive Metabolites From *Chaetomium Globosum* for Biocontrol of Sclerotinia rot and Plant Growth Promotion," *Fungal Biology* 125 (2021): 167–176, https://doi.org/10.1016/j.funbio.2020.07.009.

25. A. M. Calvo, R. A. Wilson, J. W. Bok, and N. P. Keller, "Relationship Between Secondary Metabolism and Fungal Development," *Microbiology and Molecular Biology Reviews* 66 (2002): 447–459, https://doi.org/10.1128/MMBR.66.3.447-459.2002.

26. Y. Li, Z. Wang, T. Zhao, H. Li, J. Jiang, and J. Ye, "Electronic Nose for the Detection and Discrimination of Volatile Organic Compounds: Application, Challenges, and Perspectives," *TrAC Trends in Analytical Chemistry* 180 (2024): 117958, https://doi.org/10.1016/j.trac.2024.117958.

27. J.-L. Mai, W.-W. Yang, Y. Zeng, Y.-F. Guan, and S.-J. Chen, "Volatile Organic Compounds (VOCs) in Residential Indoor Air During Interior Finish Period: Sources, Variations, and Health Risks," *Hygiene and Environmental Health Advances* 9 (2024): 100087, https://doi.org/10.1016/j.heha.2023.100087.

28. S. Sironi, L. Eusebio, L. Capelli, and M. Remondini, "Renato Del Rosso, Use of an Electronic Nose for Indoor Air Quality Monitoring," *Chemical Engineering Transactions* 40 (2014): 73–78, https://doi.org/10.3303/CET1440013.

29. Y. A. Albastaki and F. Albalooshi, *Electronic Nose Technologies and Advances in Machine Olfaction*, (IGI Global, 2018), https://doi.org/10.4018/978-1-5225-3862-2.

30. D. Sun, A. Wood-Jones, W. Wang, et al., "Monitoring MVOC Profiles Over Time From Isolates of Aspergillus Flavus Using SPME GC-MS,"

Journal of Agricultural Chemistry and Environment 3 (2014): 48–63, https://doi.org/10.4236/jacen.2014.32007.

31. K. Fiedler, E. Schütz, and S. Geh, "Detection of Microbial Volatile Organic Compounds (MVOCs) Produced by Moulds on Various Materials," *International Journal of Hygiene and Environmental Health* 204 (2001): 111–121, https://doi.org/10.1078/1438-4639-00094.

32. S. Matysik, O. Herbarth, and A. Mueller, "Determination of Microbial Volatile Organic Compounds (MVOCs) by Passive Sampling Onto Charcoal Sorbents," *Chemosphere* 76 (2009): 114–119, https://doi.org/10.1016/j.chemosphere.2009.02.010.

33. E. Brunet, T. Maier, G. C. Mutinati, et al., "Comparison of the Gas Sensing Performance of SnO2 Thin Film and SnO2 Nanowire Sensors," *Sensors and Actuators B: Chemical* 165 (2012): 110–118, https://doi.org/10.1016/j.snb.2012.02.025.

34. G. Korotchenkov, V. Brynzari, and S. Dmitriev, "Electrical Behavior of SnO2 Thin Films in Humid Atmosphere," *Sensors and Actuators B: Chemical* 54 (1999): 197–201, https://doi.org/10.1016/S0925-4005(99)00016-7.

35. S. V. Kalinin, J. Shin, S. Jesse, et al., "Electronic Transport Imaging in a Multiwire SnO2 Chemical Field-Effect Transistor Device," *Journal of Applied Physics* 98 (2005): 044503, https://doi.org/10.1063/1.2001144.

36. H. Zhang, Z. Li, L. Liu, et al., "Enhancement of Hydrogen Monitoring Properties Based on Pd–SnO2 Composite Nanofibers," *Sensors and Actuators B: Chemical* 147 (2010): 111–115, https://doi.org/10.1016/j.snb.2010.01.056.

37. A. Borhaninia, A. Nikfarjam, and N. Salehifar, "Gas Sensing Properties of SnO 2 Nanoparticles Mixed With Gold Nanoparticles," *Transactions of Nonferrous Metals Society of China* 27 (2017): 1777–1784, https://doi.org/10.1016/S1003-6326(17)60200-0.

38. F. Benrekia, M. Attari, and M. Bouhedda, "Gas Sensors Characterization and Multilayer Perceptron (MLP) Hardware Implementation for Gas Identification Using a Field Programmable Gate Array (FPGA)," *Sensors* 13 (2013) 2967–2985, https://doi.org/10.3390/s130302967.

39. Z. Cai, E. Goo, and S. Park, "Hydrogen Sensing Performance and Its Enhanced Sensing Mechanisms of Hollow Structured-SnO2 Nanospheres Activated by Noble Metal Nanoparticles," *Journal of Materials Research and Technology* 15 (2021): 1716–1731, https://doi.org/10.1016/j.jmrt.2021.09.022.

40. J.-H. Kim, A. Mirzaei, H. W. Kim, and S. S. Kim, "Improving the Hydrogen Sensing Properties of SnO2 Nanowire-Based Conductometric Sensors by Pd-Decoration," *Sensors and Actuators B: Chemical* 285 (2019): 358–367, https://doi.org/10.1016/j.snb.2019.01.008.

41. R. G. Pavelko, H. Daly, C. Hardacre, A. A. Vasiliev, and E. Llobet, "Interaction of Water, Hydrogen and Their Mixtures With SnO2 Based Materials: The Role of Surface Hydroxyl Groups in Detection Mechanisms," *Physical Chemistry Chemical Physics* 12 (2010): 2639, https://doi.org/10.1039/b921665k.

42. A. Gurlo, "Interplay Between O2 and SnO2: Oxygen Ionosorption and Spectroscopic Evidence for Adsorbed Oxygen," *Chemphyschem* 7 (2006): 2041–2052, https://doi.org/10.1002/cphc.200600292.

43. A. Rubin Pedrazzo, C. Cecone, S. Morandi, M. Manzoli, P. Bracco, and M. Zanetti, "Nanosized SnO2 Prepared by Electrospinning: Influence of the Polymer on both Morphology and Microstructure," *Polymers* 13 (2021): 977, https://doi.org/10.3390/polym13060977.

44. K. Hu, F. Wang, Y. Yan, H. Liu, and Z. Shen, "One Step From Nanofiber to Functional Hybrid Structure: Pd Doped ZnO/SnO2 Heterojunction Nanofibers With Hexagonal ZnO Columns for Enhanced Low-Temperature Hydrogen Gas Sensing," *Ceramics International* 47 (2021): 15228–15236, https://doi.org/10.1016/j.ceramint.2021.02.085.

45. A. Chizhov, P. Kutukov, A. Astafiev, and M. Rumyantseva, "Photoactivated Processes on the Surface of Metal Oxides and Gas Sensitivity to Oxygen," *Sensors* 23 (2023): 1055, https://doi.org/10.3390/s23031055.

46. M. Agarwal, M. D. Balachandran, S. Shrestha, and K. Varahramyan, "SnO 2 Nanoparticle-Based Passive Capacitive Sensor for Ethylene Detection," *Journal of Nanomaterials* 2012 (2012): 1–5, https://doi.org/10.1155/2012/145406.

47. M. Adib, R. Eckstein, G. Hernandez-Sosa, M. Sommer, and U. Lemmer, "SnO2 Nanowire-Based Aerosol Jet Printed Electronic Nose as Fire Detector," *IEEE Sensors Journal* 18 (2018): 494–500, https://doi.org/10.1109/JSEN.2017.2777178.

48. S. Das and V. Jayaraman, "SnO2: A Comprehensive Review on Structures and Gas Sensors," *Progress in Materials Science* 66 (2014): 112–255, https://doi.org/10.1016/j.pmatsci.2014.06.003.

49. V. V. Sysoev, I. Kiselev, M. Frietsch, and J. Goschnick, "Temperature Gradient Effect on Gas Discrimination Power of a Metal-Oxide Thin-Film Sensor Microarray," *Sensors* 4 (2004): 37–46, https://doi.org/10.3390/s40400037.

50. L. Li, S. He, M. Liu, C. Zhang, and W. Chen, "Three-Dimensional Mesoporous Graphene Aerogel-Supported SnO2 Nanocrystals for High-Performance NO2 Gas Sensing at Low Temperature," *Analytical Chemistry* 87 (2015): 1638–1645, https://doi.org/10.1021/ac503234e.

51. E. Comini, G. Faglia, G. Sberveglieri, Z. Pan, and Z. L. Wang, "Stable and Highly Sensitive Gas Sensors Based on Semiconducting Oxide Nanobelts," *Applied Physics Letters* 81 (2002): 1869–1871, https://doi.org/10.1063/1.1504867.

52. B. Yang, Z. Zhang, C. Tian, et al., "Selective Detection of Methane by HZSM-5 Zeolite/Pd-SnO2 Gas Sensors," *Sensors and Actuators B: Chemical* 321 (2020): 128567, https://doi.org/10.1016/j.snb.2020.128567.

53. K.-I. Choi, H.-J. Kim, Y. C. Kang, and J.-H. Lee, "Ultraselective and Ultrasensitive Detection of H2S in Highly Humid Atmosphere Using CuO-Loaded SnO2 Hollow Spheres for Real-Time Diagnosis of Halitosis," *Sensors and Actuators B: Chemical* 194 (2014): 371–376, https://doi.org/10.1016/j.snb.2013.12.111.

54. M. Adib, "UV-Excited SnO2 Nanowire Based Electronic Nose," Ph.D. thesis, Karlsruher Institute of Technology (2021).

55. M. Akbari, M. Joharifar, S. Kamaei, M. A. Mohajerzadeh, and S. Mohajerzadeh, "Modeling of Spatial Growth of SnO_2 Nanowires on Silicon Substrates by VLS Technique," *Materials Research Express* 6 (2019): 095085, https://doi.org/10.1088/2053-1591/ab3250.

56. M. Adib and M. Sommer, "Live Demonstration: Printed e-Nose for Universal Applications," in 2016 IEEE SENSORS (IEEE, 2016), 1–1, https://doi.org/10.1109/ICSENS.2016.7808570.

57. C. Arnold, M. Harms, and J. Goschnick, "Air Quality Monitoring and Fire Detection With the Karlsruhe Electronic Micronose KAMINA," *IEEE Sensors Journal* 2 (2002): 179–188, https://doi.org/10.1109/JSEN.2002.800681.

58. V. V. Sysoev, V. Y. Musatov, A. A. Maschenko, et al., "Could We Apply a NeuroProcessor for Analyzing a Gas Response of Multisensor Arrays?," *AIP Conference Proceedings* 1137 (2009): 539–542, https://doi.org/10.1063/1.3156610.

59. I. Kiselev, M. Sommer, J. Kaur Mann, and V. V. Sysoev, "Employment of Electric Potential to Build a Gas-Selective Response of Metal Oxide Gas Sensor Array," *IEEE Sensors Journal* 10 (2010): 849–855, https://doi.org/10.1109/JSEN.2009.2036441.

60. C. Arnold, W. Andlauer, D. Haringer, R. Korber, and J. Goschnick, "Gas Analytical Gradient Microarrays Compromising Low Price and High Performance for Intelligent Consumer Products," in Proceedings of IEEE Sensors (IEEE, 2002) 426–429, https://doi.org/10.1109/ICSENS.2002.1037129.

61. C. Arnold, D. Haeringer, I. Kiselev, and J. Goschnick, "Sub-Surface Probe Module Equipped With the Karlsruhe Micronose KAMINA Using a Hierarchical LDA for the Recognition of Volatile Soil Pollutants," *Sensors and Actuators B: Chemical* 116 (2006): 90–94, https://doi.org/10.1016/j.snb.2005.12.068.

62. V. V. Sysoev, I. Kiselev, T. Schneider, et al., "The Gas-Sensing Characteristics of Percolating 2-D SnO[sub 2] Nanowire Mats as a Platform for Electronic Nose Devices," *AIP Conference Proceedings* 1137 (2009): 403–404, https://doi.org/10.1063/1.3156563.

63. J. Goschnick, I. Koronczi, M. Frietsch, and I. Kiselev, "Water Pollution Recognition With the Electronic Nose KAMINA," *Sensors and Actuators B: Chemical* 106 (2005): 182–186, https://doi.org/10.1016/j.snb.2004.05.055.

64. P. Kumar, R. Bhatnagar, K. Gaur, and A. Bhatnagar, "Classification of Imbalanced Data: Review of Methods and Applications," *IOP Conference Series: Materials Science and Engineering* 1099 (2021): 012077, https://doi.org/10.1088/1757-899X/1099/1/012077.

65. A. Amin, S. Anwar, A. Adnan, et al., "Comparing Oversampling Techniques to Handle the Class Imbalance Problem: A Customer Churn Prediction Case Study," *IEEE Access* 4 (2016): 7940–7957, https://doi.org/10.1109/ACCESS.2016.2619719.

66. S. Hu, Y. Liang, L. Ma, and Y. He, "Improving Classification Performance When Training Data Is Imbalanced," *International Workshop on Computer Science and Engineering* (IEEE, 2009): 13–17, https://doi.org/10.1109/WCSE.2009.756.

67. J. Xie and Z. Qiu, "The Effect of Imbalanced Data Sets on LDA: A Theoretical and Empirical Analysis," *Pattern Recognition* 40 (2007): 557–562, https://doi.org/10.1016/j.patcog.2006.01.009.

68. T. Li, S. Zhu, and M. Ogihara, "Using Discriminant Analysis for Multi-Class Classification: An Experimental Investigation," *Knowledge and Information Systems* 10 (2006): 453–472, https://doi.org/10.1007/s10115-006-0013-y.

Supporting Information

Additional supporting information can be found online in the Supporting Information section.

Supporting file: adsr70094-sup-0001-SuppMat.docx